Surface Heating and Patchiness in the Coastal Ocean off Central California During a Wind Relaxation Event

STEVEN R. RAMP AND ROLAND W. GARWOOD

Department of Oceanography, Naval Postgraduate School, Monterey, California

CURTISS O. DAVIS

Jet Propulsion Laboratory, California Institute of Technology, Pasadena

RICHARD L. SNOW

Department of Oceanography, Naval Postgraduate School, Monterey, California

The difference between the temperature of the ocean at 4-cm and 2-m depth was continuously monitored during a cruise to the coastal transition zone off Point Arena, California (38°58′N, 123°45′W), during June 1987. The two temperatures were coincident most of the time but diverged during one nearshore leg of the cruise where large temperature differences (ΔT) of up to 4.7°C were observed between the 4-cm and 2-m sensors, in areas which were separated by regions where the two temperatures were coincident as usual. The spatial scale of this "patchy" thermal structure was about 5–10 km. The Naval Postgraduate School mixed layer model (Garwood, 1977) was used to simulate the near surface stratification when forced by the observed wind stress, surface heating, and optical clarity of the water. The model produced a thin strongly stratified surface layer at stations where exceptionally high turbidity was observed but did not produce such features otherwise. This simple model could not explain the horizontal patchiness in the thermal structure, which was likely due to patchiness in the near-surface chlorophyll distributions or to submesoscale variability of the surface wind stress.

1. INTRODUCTION

The near surface stratification off Point Arena, California (38°58′N, 123°45′W), was studied on a research cruise during June 14–28, 1987 [*Ramp et al.*, this issue] as part of the Coastal Transition Zone (CTZ) Program [*CTZ Group*, 1988]. The instrumentation used was a conventional pump-through system to measure the temperature and salinity at 2-m depth, and a second temperature probe trailed near the sea surface to measure the temperature at about 4-cm depth. Surface mixed layer depths exceeded 20 m for most of the cruise, and the 4-cm and 2-m temperatures were coincident. There was one exception, however, which occurred during a period of light winds, while transiting northward on the nearshore leg of the cruise (Plate 1). (Plate 1 is shown here in black and white. The color version can be found in the separate color section in this issue.) During this leg, large temperature differences (ΔT) of up to 4.7°C were observed between the 4-cm and 2-m temperatures, in areas which were separated by regions where the two temperatures were coincident as usual. The spatial scale of this "patchy" thermal structure was about 5–10 km.

A physical description of this intense near surface stratification is presented here along with a hypothesis explaining its existence. Basically, it is proposed that the data can be explained by intense surface heating of a very turbid ocean in the presence of light wind stress, when the mixed layer depth is very shallow. The *Garwood* [1977] mixed layer

model was used to simulate the thermal structure in the upper ocean using the observed solar insolation, wind stress, and optical clarity of the water. The model successfully simulated the large ΔT when large extinction coefficients corresponding to very turbid water were used but did not reproduce them otherwise. The patchiness of the large ΔT was therefore most likely due to patchiness of the near-surface chlorophyll distribution, although submesoscale variation in the surface wind stress, a related phenomenon, may also play a role.

The data, instrument calibrations, and methods are described in section 2. The observational results are described in section 3, and the model results with discussion are presented in section 4. A summary and conclusions section follows.

2. INSTRUMENTATION AND METHODS

The near-surface stratification was observed using the difference between the 4-cm and 2-m temperatures, both of which were measured continuously throughout the cruise, averaged at 30 s intervals, and recorded along with date, time, position, and meteorological variables on the Serial ASCII Interface Loop (SAIL) data acquisition system. The 4-cm temperature was measured using a Rosemount platinum resistance thermometer which was trailed alongside the ship in a tygon tube hanging from a boom extending about 4 m outboard of the stern of the vessel (Figure 1). This sensor had an accuracy (according to the manufacturer's specifications) of ±0.005°C and a response time of about 8 s. The sensor was encased in a brass housing which provided additional thermal mass and also enough weight to make the
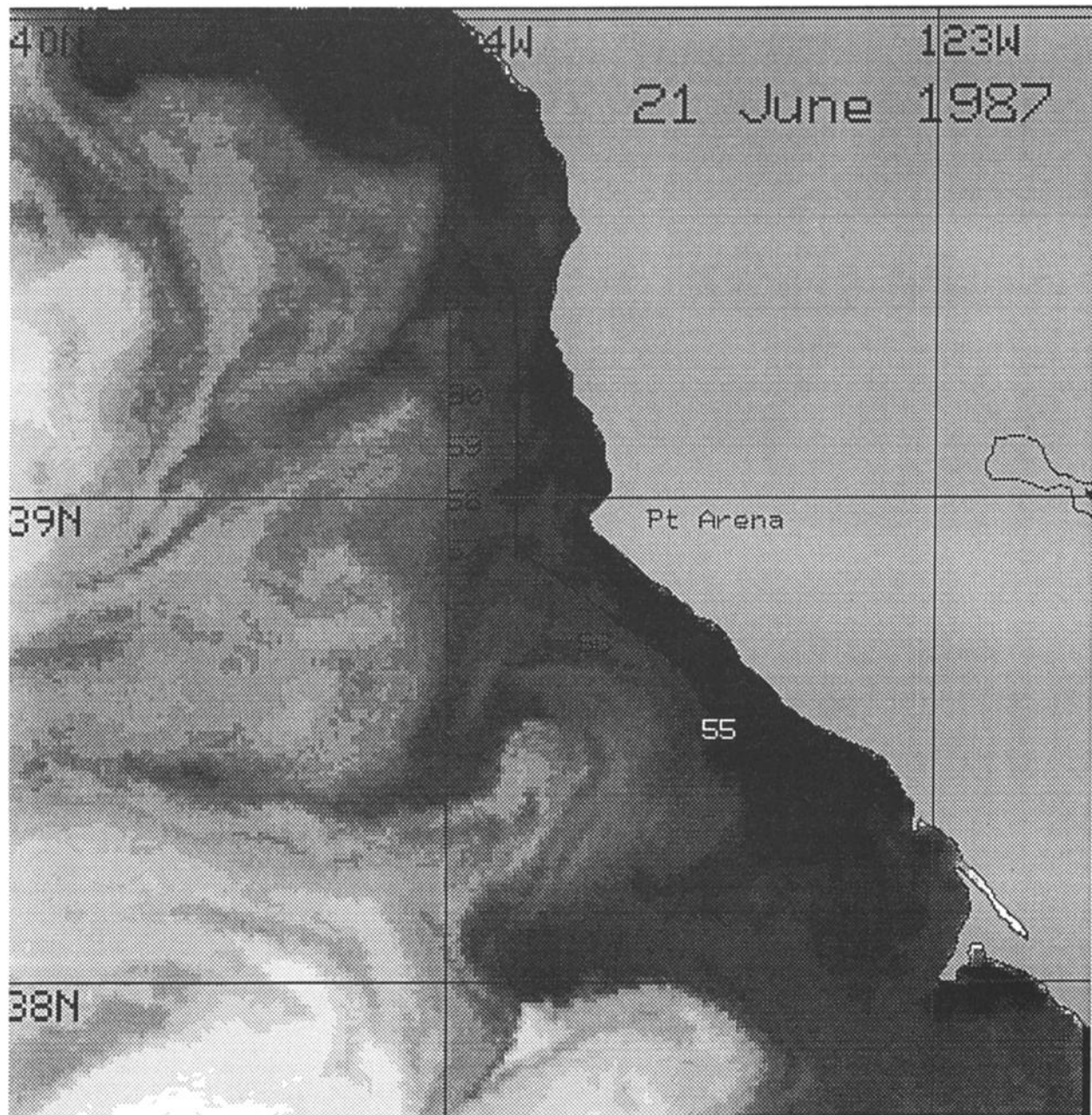
Plate 1.　A NOAA 10 satellite AVHRR sea surface temperature image from June 21, 1987, at 2003 PDT (PDT = UT − 7) with the ship's cruise track and station numbers superimposed. The darkest gray shade corresponds to the coldest water and lightest gray shade to the warmest. The stations were occupied from south to north along the coast between 1053 PDT (station 55) and 2053 PDT (station 61) on June 20. Note that the image is not synoptic with the shipboard sampling, which was done the day before. (The color version of this figure can be found in the separate color section in this issue.)

probe ride at about 4-cm depth while the ship was underway. The response time of the entire system (the sensor encased in brass, with only the tip of the thermometer exposed to the ocean) was estimated in the Naval Postgraduate School calibration laboratory to be 30–60 s.

Hours of personal observation at various vessel speeds and in many different sea states have verified that the probe does in fact ride just below the surface almost all of the time. In very heavy weather, the probe will occasionally fly out of the water for a fraction of a second, but the time constant of the measurement system is such that these small excursions

out of the water do not introduce any significant error into the measurement. The probe also rides out of the propeller wash and well away from any other water outlets from the vessel. When the ship is stopped, the probe sinks to a depth of about 1 m, so that all data from times when the ship was stopped have been deleted from the data set used in the results which follow.

The 2-m temperature was obtained by pumping water from an intake port on the ship's hull at a depth of about 2 m to an onboard sea chest and then through about 2 m of piping to the sensor. The flow rate of the water past the sensor was
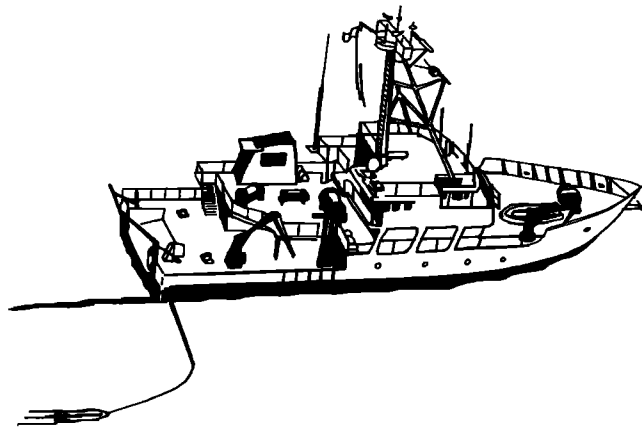
Fig. 1. Schematic drawing of the research vessel *Point Sur* showing the location of the boom probe used to measure the temperature of the ocean at about 4-cm depth. The boom extends approximately 4 m outboard of the vessel, and the probe rides about 4 cm below the surface when the ship is underway.

monitored continuously in the ship's laboratory and varied between 4 and 5 L min^{-1} depending on the status of the filters in the system which were cleaned daily. The water temperature in the 2-m system was measured by a Sea-Bird model SBE-3 oceanographic thermometer with an accuracy of ±0.003°C and a response time of 72 ms.

Both sensors were calibrated before and after the cruise. Calibration samples were obtained at 1.000°C intervals between 1.000° and 20.000°C. During the precruise calibration, the sensors produced identical output values to within their stated accuracy. The postcalibration showed that sensor drift was nonexistent for the 2-m sensor, and the 4-cm sensor drifted about 0.11°C toward cooler temperatures.

The expectation was that the 4-cm and 2-m temperatures should be coincident most of the time; however, a nearly constant offset was observed with the 2-m temperature about 0.1°C warmer than the 4-cm temperature. This offset was presumed due to heating in the engine room experienced by the water as it flowed through the piping between the intake port and the Sea-Bird temperature sensor. Evidence that the 2-m temperature was too warm was also provided by comparing the 2-m data from the conductivity-temperature-depth (CTD) instrument (a Neil Brown Instrument Systems Mark IIIB) with the 2-m temperatures from the sea chest. There was once again a mean offset between these two sensors of 0.124°C, with the sea chest sensor returning the warmer value. To obtain a more quantitative estimate of this artificial temperature offset, the data were examined during June 21–22, 1987, when winds from the northwest increased to gale force and the mixed layer deepened to 40 m depth, leaving no doubt that the upper 2-m layer of the ocean was well mixed during this time. The 4-cm and 2-m temperatures were offset by a mean value of 0.11°C with a standard deviation of 0.029°C. Based on these results, 0.11°C was subtracted from the 2-m temperatures for the entire cruise to eliminate the offset between the two measurement systems.

The shipboard winds were measured using an R. M. Young anemometer mounted at 10 m height on the ship's mast. This instrument had a speed threshold of 0.7 m s^{-1}, a direction threshold of 1.0 m s^{-1}, directional accuracy of ±5° and speed accuracy of ±0.5 m s^{-1}. Air and dew point

temperatures were observed using a General Eastern Model 1200 automatic optical/condensation hygrometer, also mounted on the ship's mast. The nominal accuracy of both these temperatures as stated by the manufacturer is ±0.2°C. Short and long wave solar insolation were observed throughout the cruise using Eppley model PSP and PIR precision calibrated pyranometers, mounted on the flying bridge away from shadowing by other equipment. All insolation variables were assumed to be uniform over the observed area, which seems reasonable for a short (80 km) transect. This assumption also agrees with results from the nearby Coastal Ocean Dynamics Experiment (CODE) where the net surface heat fluxes calculated at four meteorological buoys separated by about 60 km were found to have a very high correlation [*Lentz*, 1987]. All of the above data were collected as 30-s averages and recorded on the SAIL data acquisition system.

Water column optical data were collected with an updated version of the Bio-Optical Profiling System (BOPS) [*Smith et al.*, 1984]. The heart of the BOPS is a Biospherical Instruments MER-1048 spectroradiometer which measures upwelling and downwelling spectral irradiance and upwelling spectral radiance. The spectroradiometer also has sensors for photosynthetically available radiation (PAR), depth, tilt, and roll. In addition, temperature and conductivity are measured with a Sea-Bird CTD, chlorophyll fluorescence is measured with a Sea Tech fluorometer and beam transmission with a Sea Tech 25-cm transmissometer. The MER-1048 acquires data 16 times a second, averages it to four records a second, and sends it to a computer which stores the data. The BOPS data were filtered to remove obvious data spikes and a depth aberration which occurred at 95 m and then binned into 1-m averages.

At selected stations (55, 56, and 59 on this transect), extracted chlorophyll and phaeopigments were measured in water samples taken with the CTD rosette sampler immediately before or after the optical profile. Water samples (100 mL) were filtered on Whatman GF/F filters. Samples were extracted in 10 mL of acetone in the dark at −20°C for 24 hours and then measured in a Turner Designs model 10-005 fluorometer calibrated with pure chlorophyll (Sigma Chemical Company). Samples were remeasured after acidification with one drop of 5% HCl and chlorophyll and phaeopigments were calculated according to *Strickland and Parsons* [1972]. The extracted chlorophyll + phaeopigment values were used to calibrate the Sea Tech fluorometer data ($n = 27$, chl + phaeo = 0.236 + 0.127 fluor, $r^2 = 0.77$).

Beam transmissometer (25-cm path length, 660-nm wavelength) data were recorded as percent transmission (%T). The attenuation of a beam of light is defined by [*Jerlov*, 1976].

$$c = a + b$$

and

$$T = e^{-cx}$$

where

c beam attenuation coefficient, m^{-1};
a absorption coefficient
b total scattering coefficient;
T fraction of light transmitted over path length x.

For this data set, c was calculated from the following equation which follows immediately from the above with $x = 0.25$ m:

$$c = -4 \ln (\%T/100)$$

PAR was measured with a 2π collector located on top of the spectroradiometer. The extinction coefficient for PAR, k_{PAR}, was calculated from the 1-m binned data using

$$k_{PAR} = \Delta z^{-1} \ln (PAR_z/PAR_{z + \Delta z})$$

where PAR_z is the photosynthetically available radiation at depth z and $PAR_{z+\Delta z}$ is the same quantity at depth $z + \Delta z$.

For each station, k_{PAR} was calculated at 1-m intervals and as an average for the top 5 m. Calculating k_{PAR} from shipboard measurements of PAR from the top few meters is difficult because ship motion and surface waves cause the light field to vary rapidly when the instrument package is in the first few meters. Reflection off the ship's hull in the top few meters and the ship's shadow at slightly greater depths can also cause artifacts [Smith and Baker, 1984, 1986; Gordon, 1985]. Since k_{PAR} is calculated from the difference between successive PAR measurements, it is extremely sensitive to small errors in the PAR measurements.

Because of these potential artifacts in k_{PAR} calculated from direct measurements we also used an alternate approach calculating k_{PAR} from the chlorophyll measurements (which are not affected by these problems) according to the model of Morel [1988]. The model assumes that the extinction of light is due to the water itself and to phytoplankton and related detritus (case I waters). The beam transmission data indicate that this is a valid assumption for the surface waters off Point Arena. There was some evidence of resuspended sediments near the bottom but no indication that this sediment reached the upper 40 m. Morel's model is an empirical fit to data from 176 stations which yields

$$k(\lambda) = k_w(\lambda) + \chi_c \, chl^{e(\lambda)}$$

where chl is the chlorophyll + phaeopigments concentration (mg m^{-3}) and the extinction coefficient for water $k_w(\lambda)$, the coefficient χ_c and the exponent $e(\lambda)$ are from Table 2 of Morel [1988]. The value of k_{PAR} is found by integrating $k(\lambda)$ over the wavelengths 400–700 nm.

3. RESULTS

The key observational results are shown by 1-km averages of the air temperature, 4-cm temperature, 2-m temperature, and wind speed at 10-m height as a function of distance (Figure 2) as the ship steamed northward along the coast (Plate 1). The start and stop times on the plot (and all time references subsequently) are given in local time (Pacific Daylight Time, PDT = UT − 7) to facilitate easy comparison with diurnal heating effects. The 4-cm and 2-m temperatures began to diverge in early afternoon, and the difference between the two became greater as the 4-cm temperature rose through four intermediate peaks, each warmer than the one before, until reaching a maximum temperature of 16.23°C at km 52 (1606 PDT). The difference between the 4-cm and 2-m temperatures also reached its maximum of 4.7°C at this time. Near km 43, the 4-cm temperature dropped suddenly to less than 11°C and became nearly coincident with the 2-m temperature. The 4-cm temperature
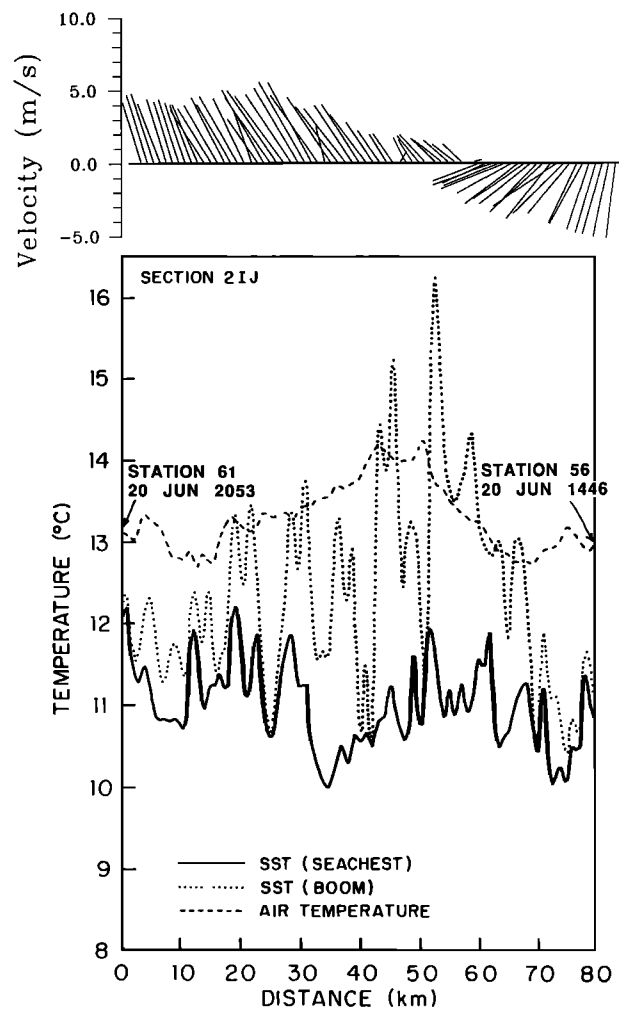

Fig. 2. The 1-km averages of air temperature, 4-cm temperature (boom), 2-m temperature (seachest), and wind velocity at 10 m height (north up) as a function of distance between stations 56 and 61 (Plate 1) showing the large differences between the 4-cm and 2-m temperature that were observed along this transect. The view is onshore with station 56 (southeast) on the right and station 61 (northwest) on the left. The x axis is not a smooth function of time, since the ship was starting and stopping, but the start and stop times of the transect are indicated (Pacific Daylight Time (PDT)) to give an approximate idea of when the sampling took place. Data from times when the ship was stopped have been edited from the plot (see text).

then rose again to 15.17°C near km 46, a value which was 4.15°C greater than the 2-m temperature. This pattern of rise and fall of the 4-cm temperature at 5–10 km scales continued along the rest of the leg. Near km 28, the two temperatures were once again coincident, and subsequently, they separated again by km 22, where the 4-cm temperature was 12.7°C and the ΔT was 0.7°C. The temperatures at the two depths converged as the ship approached the end of the leg and remained the same for the remainder of the cruise. The 4-cm temperature, the 2-m temperature, and the temperature difference $T_{4\text{-cm}} - T_{2\text{-m}}$ from the points along the transect where the two measurements diverged (Table 1) show the pattern of both $T_{4\text{-cm}}$ and ΔT increasing then decreasing with time.

The shipboard winds (Figure 2) were out of the northeast at less than 5 m s^{-1} from km 60 to 80, were near 0 m s^{-1} in late afternoon near km 60, and then blew out of the southeast

TABLE 1. The 4-cm Temperature, 2-m Temperature, and $T_{4\text{-cm}}$ − $T_{2\text{-m}}$ at Selected Points Along the Section Shown in Figure 2

Time, PDT	$T_{4\text{-cm}}$, °C	$T_{2\text{-m}}$, °C	ΔT, °C
1428	11.52	11.18	0.34
1501	11.81	11.31	0.50
1516	13.00	11.26	1.74
1547	14.29	11.33	2.96
1606	16.23	11.52	4.71
1654	15.17	11.02	4.15
1744	13.13	10.59	2.54
1806	13.77	11.34	2.43
1910	13.42	11.50	1.92
1950	12.39	11.31	1.08
2028	12.28	11.24	1.04
2042	12.32	12.25	0.06

at less than 5 m s^{-1} for the rest of the transect. The wind plot does not show any evidence of variability on the same 5–10 km scales as the surface temperature patchiness. The wind direction relative to the coastline was always offshore (Figure 3), which may explain why the air was warmer than the sea surface by 1°–2°C along the transect (Figure 2), which contributed to the stability and low wind speeds in the atmospheric surface layer. The shipboard wind observations cannot distinguish spatial from temporal variability: Figure 3 does not reveal whether the winds were southward south of Point Arena and northward to the north or whether a shift from southward to northward winds occurred over the entire area while the transect was being made.

We first present a simple calculation to verify our contention that the solar insolation on June 20 was sufficient to raise the temperature of the upper 2 m of ocean by 4.7°C.
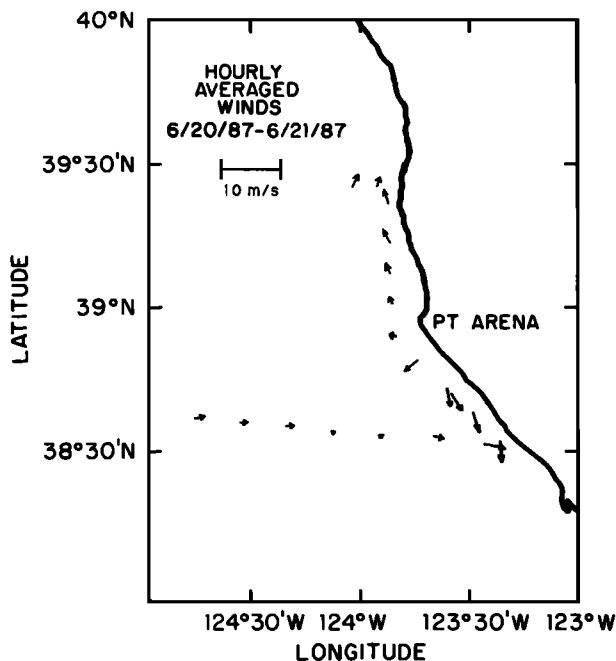

Fig. 3. Plan view of the vector winds in the study region during the approaching offshore leg and along the coast near Point Arena. Vector magnitudes (in meters per second) are indicated by the scale in the heading.

Discussion of surface patchiness will be deferred until later. The heat budget at the ocean's surface is

$$Q_0 = (1 - \alpha)Q_S + Q_L - Q_B - (Q_E + Q_H) \qquad (1)$$

where

Q_0 net heat flux;
Q_S solar shortwave radiation;
Q_L incoming longwave radiation;
Q_B longwave back radiation from the sea;
Q_E evaporative/latent heat flux;
Q_H sensible heat flux;
α albedo (reflected shortwave radiation).

Horizontal advection was assumed negligible over the 6-hour observation period. The units of Q are watts per square meter. The albedo varies principally with solar altitude and sea state. Within 40° of the equator, the minimum (cloud-free) albedo over most of the ocean is below 0.1, with average values between 0.15 and 0.30 [Gill, 1982]. Due to the short time period involved and anomalous calm, clear weather conditions encountered, an estimated value of 0.1 is used for α. This is also consistent with the albedo of 0.07 used for heat budget studies in the CODE region near Point Arena [Lentz, 1987]. Values for Q_S and Q_L were measured directly using the precision pyranometers described earlier. Q_B was estimated using Stephan's law for blackbody radiation:

$$Q_B = \varepsilon \sigma T_S^4 \qquad (2)$$

where T_S is absolute sea surface temperature (°K), $\sigma = 5.67 \times 10^{-8}$ W m^{-2} °K^{-4} (Stephan's constant), and ε is emissivity constant ≈ 1 [Large et al., 1986].

The surface fluxes were calculated with the bulk aerodynamic method following Large and Pond [1982]:

$$\tau = \rho_a \overline{|v'w'|} = \rho_a C_D |\Delta u|^2 \qquad (3)$$

$$Q_E = L_E \overline{w'q'}|_0 = L_E C_E |\Delta u| \Delta q \qquad (4)$$

$$Q_H = \rho_a C_{pa} \overline{w'T'}|_0 = \rho_a C_{pa} |\Delta u| \Delta T \qquad (5)$$

where the bulk coefficients C_D and C_E are corrected for atmospheric stability. In these equations, Δu, Δq, and ΔT are the differences in velocity, humidity, and temperature between the sea surface and the 10-m height above the surface. The values of air density (ρ_a), atmospheric specific heat (C_{pa}), and latent heat of vaporization (L_E) are held constant at representative values.

From the wind stress, the water surface friction velocity is

$$u_* = (\tau/\rho_o)^{1/2} \qquad (6)$$

where $\rho_o = 1026$ kg m^{-3} is a representative seawater density.

The observed and calculated heat flux components (Table 2) for the 0430 to 1630 PDT time period on June 20, 1987, are as one would expect for the location and season under light winds: The incoming and outgoing longwave radiation were in near balance, the latent and sensible fluxes were small, and the net flux was dominated by the shortwave solar insolation. Integrating the net heat flux over time between 0730 (the first positive value) to 1630 PDT gives a value of $Q_0 \Delta t = 5.16 \times 10^6$ cal m^{-2}, the total heat added to the water

TABLE 2. Observed and Calculated Terms in the Heat Flux Equation as a Function of Local
Time (UT − 7) on June 20, 1987

Time, PDT	Q_S	Q_L	Q_B	Q_E	Q_H	Q_0
0430	0.0	359.5	378.2	13.8	23.4	−55.9
0530	0.4	356.9	378.5	11.7	19.8	−41.0
0630	23.8	349.7	377.0	11.9	20.1	−37.8
0730	88.7	347.2	373.3	6.4	−10.7	58.1
0830	187.6	360.2	370.8	1.5	2.6	154.2
0930	382.0	354.6	370.8	2.2	3.7	321.7
1030	691.1	330.4	363.2	1.9	−3.7	591.0
1130	999.0	328.0	362.7	9.3	−15.7	870.2
1230	999.0	345.7	365.7	14.2	−24.1	889.0
1330	990.0	349.0	368.8	16.7	−28.3	882.8
1430	980.0	335.9	369.1	14.7	−24.8	858.9
1530	999.0	349.4	378.8	27.4	2.6	839.7
1630	591.9	365.0	379.3	10.5	−17.7	525.7

The terms are defined in the text, and all units are in watts per square meter. The Q_S values of 999.0 between 1130 and 1530 PDT indicate that the instrument was pegged at its highest reading.

column per square meter of surface area during the heating day on June 20, 1987.

The maximum difference between 4-cm and 2-m temperatures of 4.7°C occurred at 1606 PDT at about the 63 km point of Figure 2, about 10 hours into the heating day. The question is, could the calculated value of Q_0 raise the temperature of the upper ocean by 4.7°C if it were trapped in a surface layer less than 2 m deep? Assuming for now that this trapping is possible (we return to this question next), a volumetric approach to the heating problem can be used to determine an effective depth of heating H. Using

$$H = Q_0 \Delta t / \rho C_p \Delta T \qquad (7)$$

and the values $Q_0 \Delta t = 5.16 \times 10^6$ cal m^{-2}, $\rho = 1.026$ g cm^{-3}, $\Delta T = 4.7°C$, and $C_p = 1.0$ cal g^{-1} °C^{-1}, the resulting value of $H = 1.07$ m. This effective depth is almost at the middepth between the 4-cm and 2-m sensors and indicates that sufficient solar insolation was available to account for the observed temperature difference between the two sensors, providing it was trapped in a very shallow layer.

Two conditions must be met for this to occur: First, a very shallow turbulent mixed layer is required (less than 2-m deep) and second, the water column must be quite turbid, to maximize the absorption of solar radiation in the shallow mixed layer. Optical casts were taken at stations 55, 56, and 59 (Plate 1) before and during the time when the large near-surface temperature differences were observed and show very large differences in the chlorophyll content and transmissivity of the water column. Station 55 at the southern end of the transect was taken at 1116 PDT before the large differences occurred. The water column had a very weak subsurface chlorophyll maximum (Figure 4a), not indicative of a large phytoplankton bloom. Transmissivity (Figure 4b) was nearly uniform in the surface waters, with Beam C values ranging from 0.91 to 0.96 m^{-1} and the 1% light level at 32 m. There was a bottom nephaloid layer below 60 m at station 55 and 85 m at station 56 (Figure 4b) which did not affect processes near the surface. Station 55 can be considered a "control" station where conditions are approximately "normal" for the coastal ocean when an intense phytoplankton bloom is not occurring. Station 56 was obtained during early afternoon (1335 PDT), still prior to

the time when the large temperature differences were observed. There was a significant subsurface chlorophyll maximum (6.15 mg m^{-3} at 8 m versus 2.1 mg m^{-3} at the surface) which resulted in a slightly reduced transmissivity ($c = 1.24$ m^{-1}) of the surface waters relative to station 55. The 1% light level occurred at 21 m depth, noticeably shallower in the water column than station 55. Station 59 was taken at 1828 PDT, after the time when the maximum near-surface temperature differences were observed but while the phenomenon was still apparent. There was a large near-surface (upper 20 m) chlorophyll maximum at this station, one of the largest observed at any time during the entire cruise. Chlorophyll plus phaeopigments were 7.62 mg m^{-3} at the surface, with a maximum value of 8.36 mg m^{-3} at 8 m. A drop in transmissivity was associated with these high values near the surface: Beam C was 2.66 m^{-1} for the top 10 m, and the 1% light level was at about 12 m. While the data are insufficient to make rigorous correlations between near-surface chlorophyll and transmissivity values and the large temperature differences observed across the upper 2 m of the
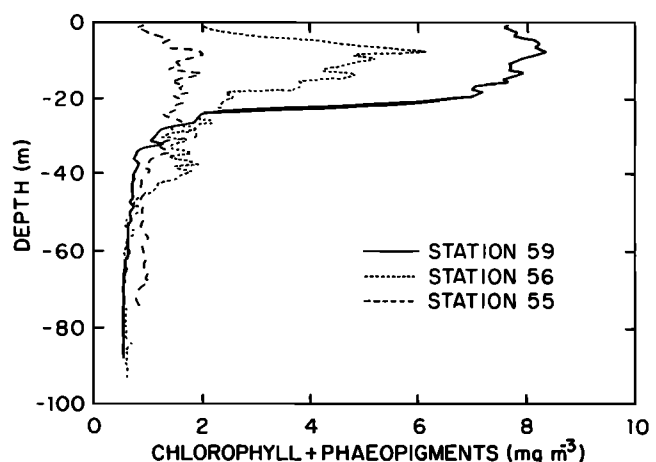

Fig. 4a. Total pigment (chlorophyll + phaeopigment) as a function of depth for stations 55, 56, and 59 (Plate 1). The maximum observed temperature differences between the 4-cm and 2-m probes were observed between stations 56 and 59.
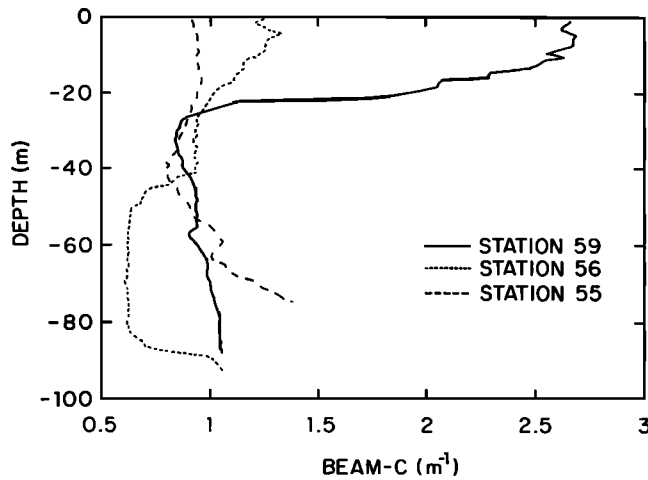
Fig. 4b. Beam C values from the Sea Tech 25-cm transmissometer as a function of depth for stations 55, 56, and 59 (Plate 1). The maximum observed temperature differences between the 4-cm and 2-m probes were observed between stations 56 and 59. The high near-surface Beam C values at station 59 correspond to the high chlorophyll + phaeopigment levels in Figure 4a.

water column, it seems fair to say that the water at station 59 (where the surface warming was observed) was uncommonly turbid, which may be necessary for the phenomenon to occur. The chlorophyll variability (Figure 4a) is likely spatial rather than temporal. Stations 55 and 59 were separated by less than 8 hours in time, which, given the known growth rates for the phytoplankton species in the region [Davis, 1982], is insufficient time for the observed changes to have occurred due to in situ phytoplankton growth and reproduction.

The extinction coefficients from the measured PAR profiles and from the chlorophyll plus phaeopigments data using the empirical model of Morel [1988] were calculated as described in section 2. As discussed previously, there are numerous difficulties making in situ measurements of PAR in the upper few meters. The k_{PAR} values calculated at 1-m intervals were quite erratic, and an average value for the upper 5 m was used. The results of the two methods compared well (Table 3) with measured values ranging from 0.24 to 0.47 m^{-1}, and modelled values ranging from 0.22 to 0.40 m^{-1}, at stations 55–59, respectively.

TABLE 3. Values of Chlorophyll + Phaeopigments at 1 m, Average k_{PAR} From the Measured PAR Values Averaged Over the Top 5 m, and k_{PAR} From the Chlorophyll + Phaeopigment Value for the Top Meter Calculated Using the Model of Morel [1988]

Station	chl + phaeo, mg m^{-3}	k_{PAR}, m^{-1}	
		Measured	Modelled
55	0.99	0.24	0.22
56	2.09	0.19	0.26
59	7.62	0.47	0.40

4. Discussion

4.1. Model Results

To understand the physics of the observed surface warming, the evolution of the thermal structure of the upper ocean was simulated using the Naval Postgraduate School (NPS) mixed layer model. This is a numerical solution of the bulk mixed layer model of Garwood [1977] based on an integrated form of the turbulent kinetic energy (TKE) budget. The assumption is made that the turbulence is sufficient to mix all the water properties thoroughly within the mixed layer. The basic physics consists of a balance between turbulent kinetic energy generated by wind stress at the surface and dampened by the buoyancy flux, entrainment from below, and viscous dissipation. Horizontal advection is neglected here. The model simulates temperature as a function of depth and time [$T(z, t)$] at a single geographical location and has been tested objectively by third parties against other models in comparison with observations [Martin, 1985; Gaspar, 1988; McCormick and Meadows, 1988].

The model inputs were from the shipboard sensors, assuming atmospheric length scales sufficiently large to justify the use of the wind and heat flux data in a single-point model; that is, these data were treated as time series at a single point. The downward irradiance in the model was parameterized using a double exponential formulation which allows for the preferential absorption of the longer wavelengths at shallower depths. The equation used is

$$I(z) = I_0[R \exp (\zeta_1 z) + (1 - R) \exp (\zeta_2 z)] \qquad (8)$$

where $I_0 = I(0)$ is the surface insolation, ζ_1^{-1} and ζ_2^{-1} are attenuation lengths, and R is an empirical constant equal to 0.5. Several model runs were made in which ζ_2 was kept constant at 0.083 m^{-1} and ζ_1 was varied, to simulate what the ship would observe as it steamed between water masses with different optical characteristics. We assumed that the coefficients did not vary temporally within each patch. Model runs with $\zeta_1 = 0.2$ m^{-1}, similar to the observed values at stations 55 and 56 (Table 3) did not produce the large ΔT observed near the surface. When ζ_1 was changed to 0.5 m^{-1} (corresponding to a secci disk depth of only 2 m) similar to the observed values at station 59 (Table 3), large ΔT were produced which were similar in magnitude to those actually observed (Table 1). The total heat input (Figure 5a) peaked at about 800 W m^{-2} at about 1300 hours. The wind stress, expressed as the friction velocity u_* (Figure 5b) was near 0 at 0700–0800, peaked at about 0.45 m^2 s^{-2} about an hour later, and returned to near zero again between 1600 and 1800. The turbulent boundary layer depth (Figure 5c) was initialized to 15 m during the night, and then was reduced to nearly zero (0.2 m) from 0700 to 0800, deepened to 6–7 m in response to the increase in u_* in early morning and midday, and then returned to nearly zero in late afternoon between 1600 and 1800 in response to increased heating and the diminishing winds. During the late afternoon calm, when the turbulent boundary layer nearly vanished, the model produced a strong shallow thermocline at less than 0.5 m depth (Figure 5d), with ΔT across it exceeding 2.5°C. The model temperature differences $T_0 - T_{2-m}$ (Figure 5e) were calculated to simplify comparison with the observed temperature differences $T_{4-cm} - T_{2-m}$ (Table 1). The maximum model-generated ΔT was about 2.75°C and occurred at about 1600
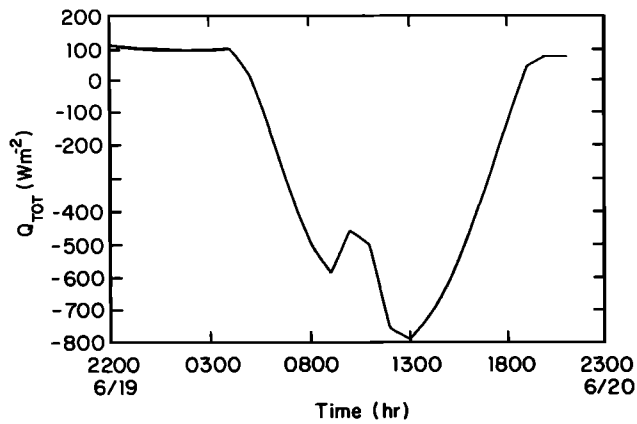
Fig. 5a.   Net surface heat flux (W m^{-2}) versus time. Maximum net heating at about 1300 PDT is after local noon because of reduced wind speeds and increased air temperature.
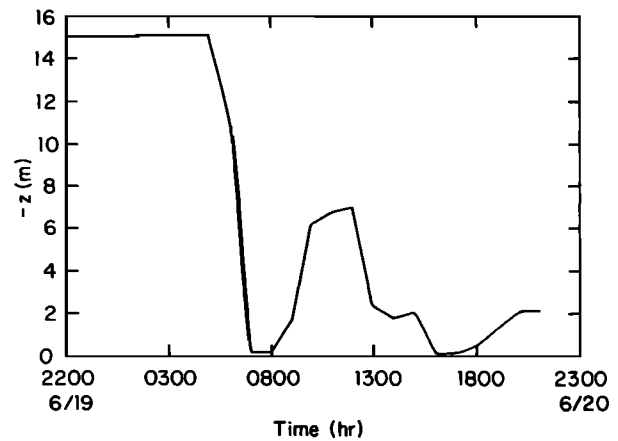

Fig. 5c.   Model computed mixed layer depth (m) versus time. See text for explanation.

in the late afternoon, versus 4.7°C at 1606 for the observations. The lower magnitude produced by the model can perhaps be explained by the lack of chlorophyll and Beam C data during the late afternoon. Since stations 56 and 59 were occupied at 1315 and 1810, respectively, the total chlorophyll plus phaeopigments and Beam C values were not observed concurrently with the largest ΔT and values of ζ_1 even higher than the 0.5 m^{-1} used in the model may perhaps be appropriate.

Based on the model results, we hypothesize that strong temperature gradients and high temperature differences can occur over the upper 2 m of the water column when very high turbidity, high solar insolation, and near zero wind stress prevail. The horizontal patchiness of the temperature peaks on the 10-km scale was likely due to horizontal patchiness in the near-surface chlorophyll concentrations near the upwelling center off Point Arena. When the ship was between patches, the incoming solar radiation was not trapped in the upper 2 m, and the ΔT were small or zero, but when the ship was in the high-turbidity water, the larger ΔT were observed. The amplitude of the peaks increased during late afternoon when greater Q_0 was available to heat the water. Still later in the day, when the air temperatures fell and the surface wind stress increased, the surface microlayer was dissipated by vertical mixing, and the large ΔT were no longer observed.
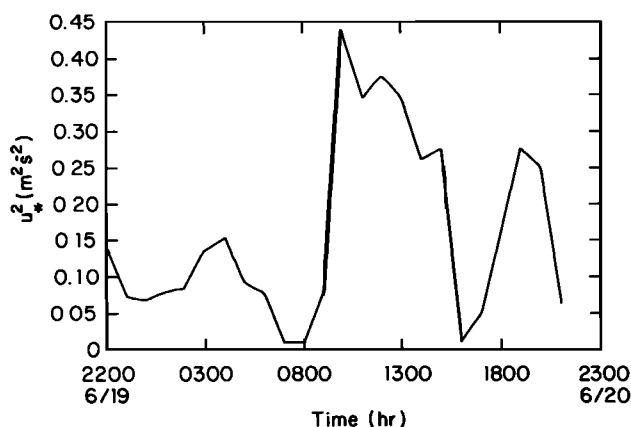
What causes patchiness in the near-surface chlorophyll distributions? One possibility is that the ship steamed through different water masses, possibly introduced by an active mesoscale eddy field in the region, which had different levels of primary productivity associated with them. A synoptic satellite image of the sea surface temperature on June 20 was not available; however, Plate 1 shows that all the stations were in a band of upwelled water near the central California coast. The image indicates minor differences in SST along the cruise track of less than 1°C. If the image is representative of conditions 24 hours earlier, then variations due to major differences in the water mass structure can be ruled out in this case. Station 55 was in the coldest and presumably most recently upwelled water, where a phytoplankton bloom had not yet been established. Station 56 was on the edge of a warm eddy but was still in the upwelled water and was quite similar to station 55 (Figure 4). Station 59 was just slightly farther offshore (about 3 km) in slightly warmer water. Organisms at this station may have had sufficient time to establish themselves and form a bloom.

This work suggests a feedback mechanism which may enhance the growth of organisms in selected patches. Light,

Fig. 5b.   Water surface friction velocity squared (m^2 s^{-2}) versus time. Note the light winds near 0700–0800 and again at 1600–1700.
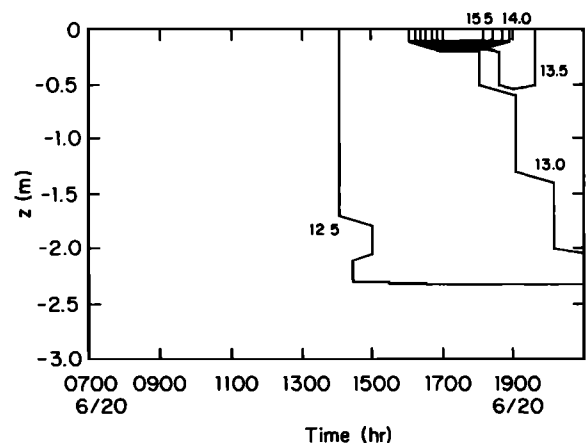

Fig. 5d.   Model simulated temperature structure, $T(t, z)$, with a 0.5°C contour interval. Vertical coordinate is meters relative to the surface, time in hours. The simulated maximum temperature of 15.5°C occurred in the top 0.1 m at about 1700 PDT. Note the expanded time scale relative to the other four plots.
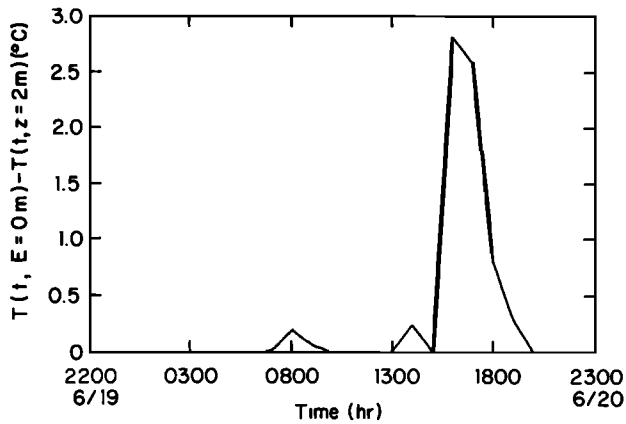
Fig. 5e. Model simulated "vertical temperature patchiness," $T(t, z = 0$ m$) - T(t, z = 2$ m$)$. This plot simulates the observed difference between the 4-cm and 2-m temperature probes.

stability, and nutrients are necessary to sustain a phytoplankton bloom. Once a patch has been started, enhanced heating and stratification (stability) will accelerate growth within the patch relative to surrounding waters, which in turn increases the surface turbidity and enhances the heating still more, which further stimulates growth, etc., and leads to strongly patchy chlorophyll distributions.

4.2. Previous Work

Previous observations of temperature differences this large over the upper 2 m of the water column are scarce. Using cleverly modified expendable bathythermograph (XBT) probes in the open ocean south of Bermuda ($28°45'$N, $68°25'$W), *Bruce and Firing* [1974] observed the development and disappearance of a shallow (1–2 m) layer that was $2°$–$3°$C warmer than the layer immediately below. These observations were also made on a windless day with strong solar insolation, which seems necessary to produce these layers. The layer was well developed late in the day (1840 PDT) but was gone by 2125. This is similar to our observations when the large ΔT disappeared by 2015. *Lewis et al.* [1983] report observations by *Schindler et al.* [1981] of differential heating in the chlorophyll maximum layer in a lake of $0.5°$C h^{-1}. Such heating rates, if persistent, could lead to temperature differences of several degrees over the course of an afternoon such as we have observed. Strong near-surface vertical temperature gradients have also been observed in an area about 35 km to the south of our observations during periods of light winds (A. Huyer, personal communication, 1990). One possible example is contained in the data report by *Fleischbein et al.* [1983] which shows a temperature gradient of $4.46°$C over the upper 10 m at their station 65.

Several investigators have studied the large diurnal variations in sea surface temperature which are sometimes observed in both satellite and in situ measurements. This is a different measure, since we are observing large vertical differences in near-surface temperature, while they are observing large temporal differences over 24 hours time. The two phenomena are perhaps related, however, since the former (trapping of heat in a very shallow layer) seems necessary for the latter. *Stramma et al.* [1986] studied large diurnal changes in sea surface temperature (SST) using advanced very high resolution radiometer (AVHRR) and

moored buoy data at the Long-Term Upper Ocean Study (LOTUS) site ($34°$N, $70°$W) between May 1982 and May 1984, and modelled these changes using the *Price et al.* [1986] mixed layer model. Price et al.'s Figure 2 shows observed temperature differences of $>2°$C between a thermistor at 0.6 m depth and a current meter at 5 m depth, for 4 consecutive days in July 1982. These large ΔT are not as extreme as those observed off Point Arena, even though the LOTUS measurements were made at a lower latitude and later in the summer. This can likely be explained as follows: 1) The clearer water offshore at the LOTUS site as compared to the CTZ study area off Point Arena will not trap as much heat in the near surface layer; and (2) the upper 0.6 m of water was unsampled, and a large fraction of the elevated temperature occurs there. The *Price et al.* [1986] model simulated differences of $3°$–$4°$C over this depth range during the same time period. This model also used the double exponential fit with the primary coefficient β_1 (= ζ_1^{-1} in our notation) determined by model fitting. They note that the model results under light wind conditions are rather sensitive to β_1.

Flament [1989] has also made observations of the horizontal and vertical structure of the surface layer under low wind conditions. Using satellite AVHRR data, he observed that diurnal warming "streaks" occurred in the California Current imagery at scales of about 50 by 4–8 km, with ΔT of $0.5°$–$1.5°$C. He also made in situ measurements during July 1985 about 100 km offshore from where our measurements were made. Winds were weak (under 1 m s^{-1}), and the sea surface was glassy, much like the conditions when our measurements were made. Using underway instrumentation, they observed horizontal scales of 2–8 km, shallow restratified upper layers 3–8 m thick, and vertical ΔT across the stratification of $0.3°$–$1.3°$C. These length scales are quite similar to ours, with ΔT substantially smaller over the upper water column. These ΔT likely represent minima, however, since the CTD did not adequately sample the upper meter of the water column where the greatest variations occur. *Flament* [1989] suggests that helical circulation rolls in the atmospheric boundary layer may be relevant to the problem, at scales of order 2–4 times the (atmospheric) boundary layer thickness. The effect of such rolls would be to cause sea surface convergence at the updrafts, divergence at the downdrafts, and a relative wind stress maximum in between. This in turn may provide a feedback mechanism in which the warm air beneath the updrafts fuels the motion (and vice versa) causing a coupled air-ocean stability problem. The stress maxima between such rolls (which must still be regarded as speculative) might cause sufficient mixing (only 2 m is needed) to erase the signal that we observed, creating the patchiness. In addition to the basic physics of heating and cooling, this mechanism might also serve to redistribute the surface concentration of phytoplankton, thereby altering ζ_1 and enhancing the surface trapping of solar insolation in the convergence zones.

4.3. Dependence of Surface Buoyancy Flux on Radiation Absorption

To evaluate the correctness of equation (8) versus a single exponential ($I(z) = I_0 \exp(\zeta z)$) or some other function for radiation absorption, one needs to evaluate the dependence of the buoyancy flux upon the function $I(z)$. For mixing processes dependent upon the intensity of the turbulence,
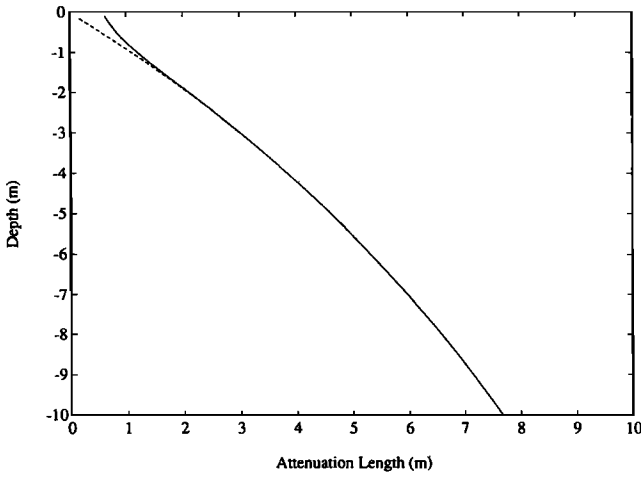
Fig. 6. The attenuation length (m) as a function of depth (m) for a double exponential function (solid curve) and a single exponential function plus a constant (dashed curve). Details of the two functions are described in the text.

the surface buoyancy flux makes a dominant contribution to the mechanical energy budget and hence to the turbulent kinetic energy. The effective downward surface buoyancy flux $(u_* b_*)$ depends upon the actual surface buoyancy flux, $\alpha g \overline{T'w'(0)}$, plus a component attributable to the absorption of solar radiation between the surface ($z = 0$) and the bottom of the mixed layer at $z = -h$ [Garwood, 1977]:

$$u_* b_* = \frac{-\alpha g \overline{T'w'(0)}}{\rho c_p} - \frac{\alpha g}{\rho c_p} \int_{-h}^{0} \left[\frac{\partial I}{\partial z} - \frac{2}{h} \int_{z}^{0} \frac{\partial I}{\partial z} d\lambda \right] dz$$

(9)

where α is the thermal expansion coefficient, T' and w' are the temperature and vertical velocity fluctuations, g is the acceleration due to gravity, and the other variables are as defined previously. If the solar radiation that penetrates the surface is approximated by the two-component function (8), the integration of (9) gives

$$u_* b_* = \frac{-\alpha g \overline{T'w'(0)}}{\rho c_p} + \frac{\alpha g I_0}{\rho c_p} R \left[1 - e^{-h\zeta_1} - \frac{2}{h\zeta_1} (1 - e^{-h\zeta_1}) \right]$$
$$+ \frac{\alpha g I_0}{\rho c_p} (1 - R) \left[1 - e^{-h\zeta_2} - \frac{2}{h\zeta_2} (1 - e^{-h\zeta_2}) \right]$$

(10)

In most open ocean circumstances, when the mixed layer depth is considerably greater than 1 m, the radiation function (10) is well approximated by assuming $\zeta_1 \sim \infty$. The plot of attenuation length versus depth (Figure 6) illustrates the difference between a double exponential function (8), versus a single exponential function plus a constant. As can be seen, when the depth of mixing is considerably greater than 1 m, the two functions are almost identical. However, when the mixing depth is very shallow, the use of the double exponential form for radiation absorption is warranted. This agrees with the results of Simpson and Dickey [1981], who found, using a modified version of the turbulence closure model of Mellor and Yamada [1974], that the double exponential formulation produced shallower mixed layers and greater surface temperatures under low wind speeds than did

the single exponential formulation. Although horizontal variability in absorption cannot be considered here because of lack of continuous observations of chlorophyll, the absorption in the top meter at three locations (Table 3) is consistent with the modelled absorption using equation (8) (Figure 6).

4.4. Compounding Effect on Mixed Layer Temperature of Radiation in Light Winds

As long as the mixed layer is shallowing, the turbulent kinetic energy budget for the mixed layer is dominated by a balance between buoyant damping, dissipation and wind stirring (shear production due to wind stress). During these times, the mixed layer shallows to a depth proportional to the Obukhov length scale,

$$L = u_*^3/(k u_* b_*)$$

(11)

where u_* is the friction velocity at the sea surface, $u_* b_*$ is the effective downward surface buoyancy flux (9), and k is von Karman's constant. With no entrainment, the local heat budget for the shallowing mixed layer at these times is simply

$$\partial \overline{T}/\partial t = Q_0/\rho C_p L.$$

(12)

If the net downward surface heat flux at the sea surface, Q_0 is caused primarily by solar radiation (possible for light winds), then L is inversely proportional to I_0, and $\partial \overline{T}/\partial t$ will be proportional to I_0^2:

$$\partial \overline{T}/\partial t \cong (k\alpha g/u_*^3)(I_0/\rho C_p)^2$$

(13)

from (10), (11), and (12) in the limit of a very turbid ocean ($\zeta_1 \sim \zeta_2 \sim \infty$). When the mixed layer again starts to entrain and deepen, this relationship will no longer be valid. However, the surface heating rate may be extreme during a period of several hours near local noon if the winds are light, explaining the 2°–3°C rise in sea surface temperature in a few hours.

5. CONCLUSIONS

Very large temperature differences were observed over the upper 2 m of the ocean near Point Arena, California, during June 1987, during a period of near-zero wind, high solar insolation, and high biological productivity. The 2-m temperatures were observed by continuously pumping seawater through an inlet on the ship's hull nominally 2 m below the surface. The 4-cm temperature was made using a simple, novel temperature probe which trails on the surface at about 4-cm depth. The two sensors were carefully calibrated in the laboratory both before and after the cruise. The two probes measured the same temperature at sea during well-mixed conditions, after subtracting 0.11°C from the 2-m temperatures to allow for heating which took place between the inlet and the sensor in the engine room.

The large temperature differences were observed while transiting north around Point Arena about 10 km offshore. Starting in early afternoon, the two temperature records began to diverge, with the 4-cm temperature far greater than the 2-m temperature. The difference between the two became greater as the 4-cm temperature rose through four intermediate peaks, each warmer than the one before, until reaching a maximum of 16.23°C versus 11.50°C for the 2-m probe, a difference of 4.7°C. The maximum difference peaks were separated by regions where the two temperatures were coincident, and the scale of this patchiness was about 5–10

km. The large differences disappeared in early evening and were not observed again.

The observational results were interpreted using the mixed layer model of *Garwood* [1977]. The model inputs (surface wind stress, solar insolation, and extinction coefficients for radiation in the sea) were all estimated using quantities observed during the cruise. The wind stress and solar insolation were measured while the ship was underway, but were considered invariant over the study area (80 km). The extinction coefficients varied spatially due primarily to patchiness in the near-surface phytoplankton distributions. This effect was simulated by specifying different extinction coefficients for different model runs and examining the magnitude of the near-surface stratification that developed. A model run using $\zeta_1 = 0.2$ m^{-1} and $\zeta_2 = 0.083$ m^{-1} did not reproduce the shallow trapped layer with the large temperature differences, however, a model run with $\zeta_1 = 0.5$ m^{-1} and $\zeta_2 = 0.083$ m^{-1} successfully simulated a very shallow (0.5 m) thermocline, with maximum ΔT across it of about $2.75°C$.

A unique aspect of this work is the observed patchiness of the large ΔT at 5–10 km scales. This simple one-dimensional model cannot reproduce the patchiness of the observations, but we suspect that this patchiness was caused by the ship steaming through regions of high phytoplankton concentration separated by regions of lower phytoplankton concentration in the upwelling zone off Point Arena. A shipboard system for continuously monitoring the surface chlorophyll distribution would have been very helpful in verifying this hypothesis, and should perhaps be added to the SAIL system as a standard feature on UNOLS vessels. Determining the cause of the phytoplankton patchiness is beyond the scope of this paper, and may be related to both biological and physical factors. Submesoscale variability of the surface wind stress, which would have occasionally mixed the upper layer to beyond 2-m depth, may also contribute to the patchiness of the observations, although we can find no evidence for this in our data set. The phytoplankton and wind patchiness may both be related to weak vertical circulations in the atmospheric boundary layer, which can only be detected by specialized instrumentation during periods of very light winds.

REFERENCES

Bruce, J. G., and E. Firing, Temperature measurements in the upper 10 m with modified expendable bathythermograph probes, *J. Geophys. Res., 79,* 4110–4111, 1974.

CTZ Group, The coastal transition zone program, *Eos Trans. AGU, 69,* 698–699, 704, 1988.

Davis, C., The importance of understanding phytoplankton life strategies in the design of enclosure experiments, in *Marine Mesocosms,* edited by G. D. Grice and M. R. Reeve, pp. 323–332, Springer-Verlag, New York, 1982.

Flament, P., AVHRR observations of the horizontal structure of the surface layer of the ocean under low wind conditions, in *Proceedings of the IGARSS'89 Conference,* pp. 318–322, Institute of Electrical Engineers, New York, 1989.

Fleischbein, J., W. E. Gilbert, and A. Huyer, Hydrographic data from the second Coastal Ocean Dynamics Experiment: R/V *Wecoma,* leg 6, 18–24 April 1982, *CODE Tech. Rep. 11,* 86 pp., Natl. Sci. Found., Washington, D. C., 1983.

Garwood, R. W., An oceanic mixed layer model capable of simulating cyclic states, *J. Phys. Oceanogr., 7,* 455–468, 1977.

Gaspar, P., Modeling the seasonal cycle of the upper ocean, *J. Phys. Oceanogr., 18,* 161–180, 1988.

Gill, A. E., *Atmosphere-Ocean Dynamics,* 652 pp., Academic, San Diego, Calif., 1982.

Gordon, H. R., Ship perturbation of irradiance measurements at sea, 1, Monte Carlo simulations, *Appl. Opt., 24,* 4172–4182, 1985.

Jerlov, N. G., *Marine Optics,* Elsevier, New York, 1976.

Large, W. G., and S. Pond, Sensible and latent heat flux measurements in the ocean, *J. Phys. Oceanogr., 12,* 464–482, 1982.

Large, W. G., J. C. McWilliams, and P. P. Niiler, Upper ocean thermal response to strong autumnal forcing of the northeast Pacific, *J. Phys. Oceanogr., 16,* 1524–1550, 1986.

Lentz, S. J., A heat budget for the northern California shelf during CODE 2, *J. Geophys. Res., 92,* 14,491–14,509, 1987.

Lewis, M. R., J. J. Cullen, and T. Platt, Phytoplankton and thermal structure in the upper ocean: Consequences of nonuniformity in chlorophyll profile, *J. Geophys. Res., 88,* 2565–2570, 1983.

Martin, P. J., Simulation of the mixed layer at OWS November and Papa with several models, *J. Geophys. Res., 90,* 903–916, 1985.

McCormick, M. J., and G. A. Meadows, An intercomparison of four mixed layer models in a shallow inland sea, *J. Geophys. Res., 93,* 6774–6788, 1988.

Mellor, G. L., and T. Yamada, A hierarchy of turbulence closure models for planetary boundary layers, *J. Atmos. Sci., 31,* 1791–1806, 1974.

Morel, A., Optical modeling of the upper ocean in relation to its biogenous matter content (case I waters), *J. Geophys. Res., 93,* 10,749–10,768, 1988.

Price, J. F., R. A. Weller and R. Pinkel, Diurnal cycling: Observations and models of the upper ocean response to diurnal heating, cooling, and wind mixing, *J. Geophys. Res., 91,* 8411–8427, 1986.

Schindler, J. E., M. C. Waldron, J. O. Eubanks, and D. L. Daugherty, Importance of particulate layer formation and internal radiation absorption in the development of the thermocline, paper presented at 44th Annual Meeting, Am. Soc. of Limnol. and Oceanogr., Milwaukee, Wis., June 1981.

Ramp, S. R., P. F. Jessen, K. H. Brink, P. P. Niiler, F. L. Daggett, and J. S. Best, The physical structure of cold filaments near Point Arena, California, during June 1987, *J. Geophys. Res.,* this issue.

Schindler, J. E., M. C. Waldron, J. O. Eubanks, and D. L. Daugherty, Importance of particulate layer formation and internal radiation absorption in the development of the thermocline, paper presented at 44th Annual Meeting, Am. Soc. of Limnol. and Oceanogr., Milwaukee, Wis., June 1981.

Simpson, J. J., and T. D. Dickey, The relationship between downward irradiance and upper ocean structure, *J. Phys. Oceanogr., 11,* 309–323, 1981.

Smith, R. C., and K. S. Baker, The analysis of ocean optical data, *Proc. SPIE Ocean Optics, VII(489),* 119–126, 1984.

Smith, R. C., and K. S. Baker, Analysis of ocean optical data II, *Proc. SPIE Ocean Opt., VII(637),* 95–107, 1986.

Smith, R. C., C. R. Booth, and J. L. Star, Oceanographic biooptical profiling system, *Appl. Opt., 23,* 2791–2797, 1984.

Stramma, L., P. Cornillon, R. A. Weller, J. F. Price, and M. G. Briscoe, Large diurnal sea surface temperature variability: Satellite and in situ measurements, *J. Phys. Oceanogr., 16,* 827–837, 1986.

Strickland, J. D. H., and T. R. Parsons, A practical handbook of seawater analysis, *J. Fish. Res. Board Can., 167,* 311 pp., 1972.

C. O. Davis, Jet Propulsion Laboratory, California Institute of Technology, 4800 Oak Grove Drive, Pasadena, CA 91109.

R. W. Garwood, S. R. Ramp, and R. L. Snow, Department of Oceanography, Naval Postgraduate School, Monterey, CA 93943.
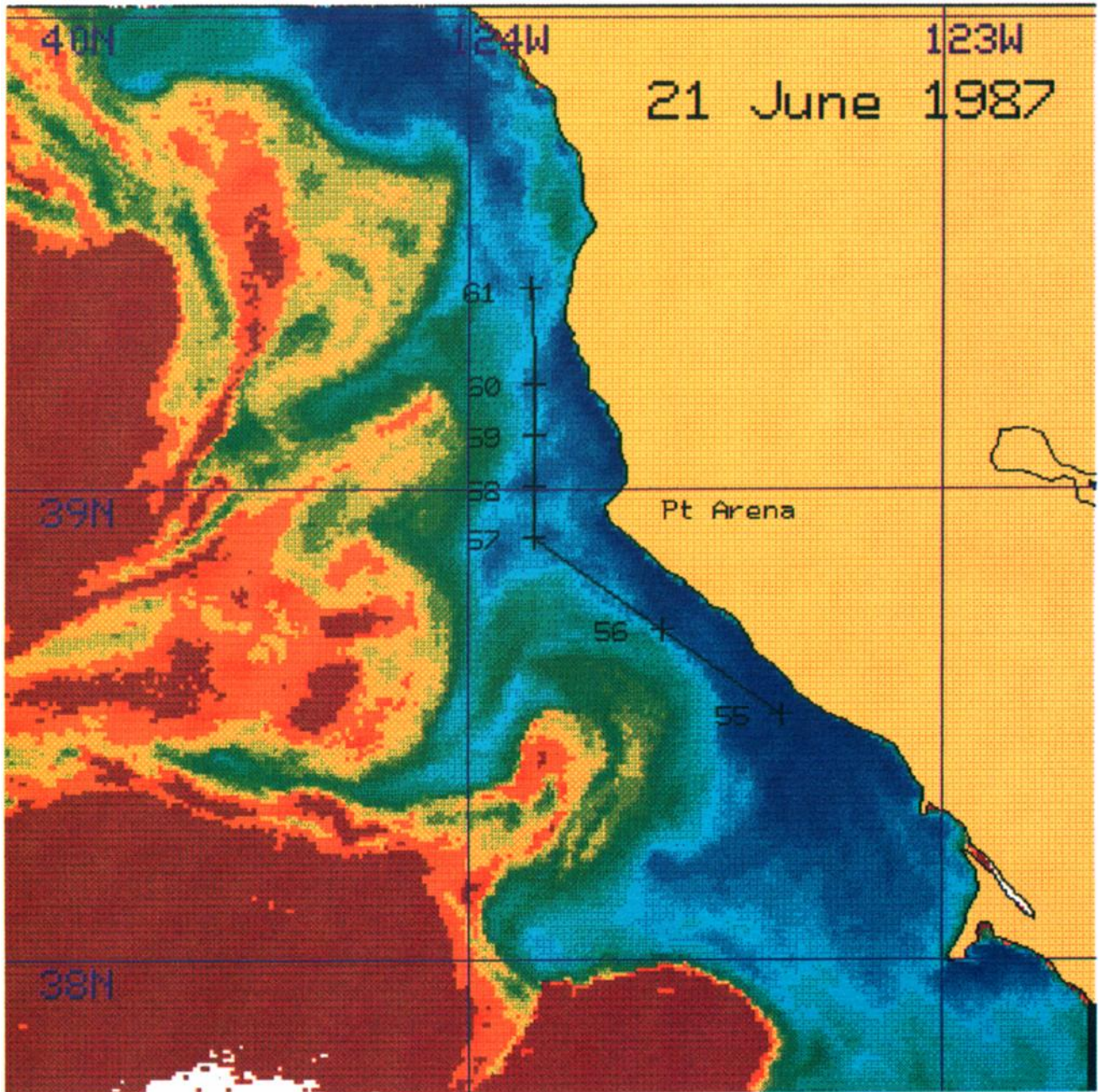
Plate 1 [*Ramp et al.*].   A NOAA 10 satellite AVHRR sea surface temperature image from June 21, 1987, at 2003 PDT (PDT = UT − 7) with the ship's cruise track and station numbers superimposed. The dark blue color corresponds to the coldest water and orange to the warmest, with light blue, green, and yellow in between. The stations were occupied from south to north along the coast between 1053 PDT (station 55) and 2053 PDT (station 61) on June 20. Note that the image is not synoptic with the shipboard sampling, which was done the day before.